Development of Full-Field X-Ray Multi-Contrast Zooming Optics

In imaging science, the zoom function plays an important role for observing the region of interest in a sample at optimal magnifications. In full-field X-ray imaging at synchrotron radiation facilities, however, the observation of samples is not always performed under optimal conditions because most experiments are conducted under fixed magnifications. To solve this problem, we developed two kinds of X-ray zooming optics: one is based on two Fresnel zone plates and the other is based on a variable zoom Bragg magnifier. We could change the magnification in the range of 25–150× with the former optics and 1–10× with the latter optics.

In imaging science, the zoom function plays an important role for observing an entire sample and/or region of interest (ROI) within a sample at the optimal magnification. In fact, optical and electron microscopes are usually equipped with a zoom function, allowing the user to identify the ROI at a low magnification and then zoom in to an optimal magnification for detailed observation. In full-field X-ray imaging at synchrotron radiation facilities, however, the observation of samples is not always performed under optimal conditions because most experiments are conducted at fixed magnifications. To solve this problem, we developed two kinds of X-ray zooming optics: one is based on two Fresnel zone plates (FZPs) [1] and the other is based on a variable zoom Bragg magnifier [2].

The optical arrangement of a zooming microscope using two FZPs with parallel beam illumination is shown in **Fig. 1(a)** [1]. The sample position is taken as the origin and the coordinate of the camera (camera length) is defined as L. Assuming that the coordinate and focal length of the first FZP are X_1 and f_1 and those of the second FZP are X_2 and f_2, then X_2 and magnification can be calculated from two lens equations using L, f_1, and f_2 as a function of X_1. This means that the magnification can be changed by placing the two FZPs at the appropriate coordinates. In parallel beam illumination, the focal point (FP) of the illumination light is located behind the first FZP. By inserting a knife edge, a phase-contrast image can be easily obtained [3]. A microscope using two FZPs was demonstrated at the BL-20B and AR-NE1A beamlines. An FZP produces both converging positive-order and diverging negative-order diffracted light, meaning that it acts as both convex and concave lenses, unlike ordinary optical lenses. Therefore, the image in **Fig. 1(a)** contains two indistinct patterns as well as the well-focused one. These patterns correspond to the images generated by minus-first-order diffraction, zeroth-order diffraction, and first-order diffraction at the second FZP, in order from the bottom. The field of view of the well-focused image generated by the minus-first-order diffraction is large, although it is partially limited due to the overlap with that by the zeroth-order diffraction. The Siemens pattern zoomed to various magnifications of 25–150× in the optical arrangement with two FZPs at 14.4 keV is shown in **Fig. 1(b)**. It was confirmed that the magnification can be continuously changed even with the sample and camera fixed. The proposed microscope enables multi-contrast zooming, which is useful for soft-tissue observation of biological samples.

Figure 2 schematically shows the X-ray zooming optics for analyzer-based multi-contrast computed tomography (CT) [2]. This optics consists of a collimator and an analyzer with a sample placed between them. The analyzer also serves as a variable zoom Bragg magnifier. The magnification can be controlled by changing the azimuth angle of the analyzer/magnifier. Proof-of-principle experiments of this optics were carried out at the vertical wiggler beamline BL-14B. The incident monochromatic beam (λ = 0.112 nm) was collimated and expanded in the horizontal plane by a Si (220) asymmetric crystal. The beam that was transmitted through the sample was analyzed and magnified in the horizontal direction by a Si (220) asymmetric crystal. As a sample, we observed the stem of Japanese pampas grass (*Miscanthus sinensis*), the diameter of which was about 2.3 mm. The analyzer was scanned through the Bragg diffraction condition in 1.25 arcsec steps. The number of measured analyzer angles was 41. At each analyzer angle, the sample was rotated around the vertical axis from 0° to 180° in 1° steps for acquiring the CT data set. The exposure time for each image was 1 s. First, we observed the sample at 1×, and then zoomed in until we reached the optimal magnification of 10×. The tri-modal contrast cross-sectional images of the sample were obtained as shown in **Figs. 3 (a)–(f)**. It can be clearly seen that for each contrast (apparent-absorption, phase, and USAXS), the vascular bundles and epidermis are more clearly depicted at 10× than at 1×.

These results open up new possibilities for observing an entire sample or ROIs within a sample at optimal magnification, and are expected to be useful for materials science, condensed matter physics, archaeology, and biomedical science.

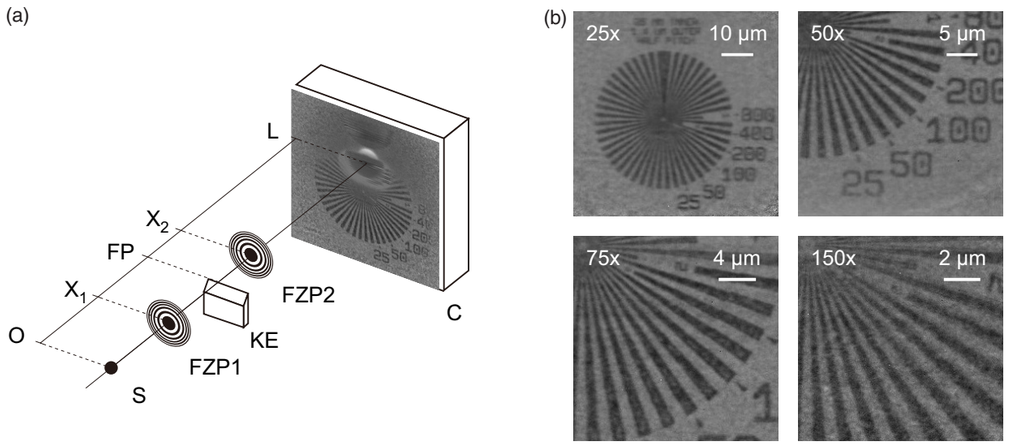

Figure 1: (a) Optical layout of the X-ray microscope with two FZPs and **(b)** zoom view of the Siemens pattern. The variables in **(a)** are defined in the main text. The abbreviations are as follows: S, sample; FZP1 and FZP2, Fresnel zone plates; KE, knife edge; and C, camera. Each figure in **(b)** was adjusted to have the same pixel size and image orientation.

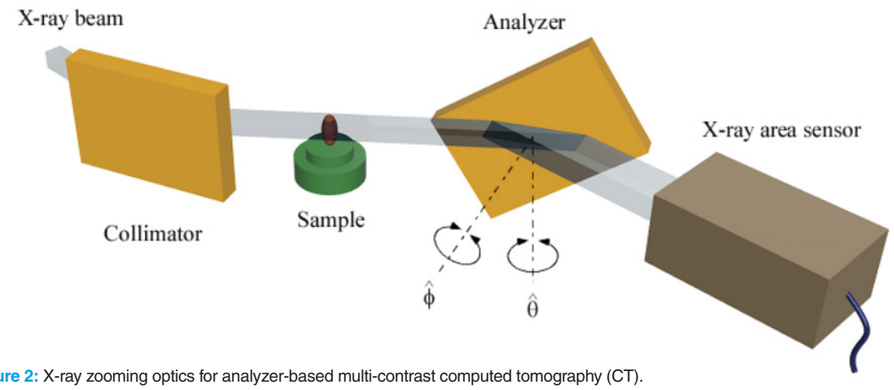

Figure 2: X-ray zooming optics for analyzer-based multi-contrast computed tomography (CT).

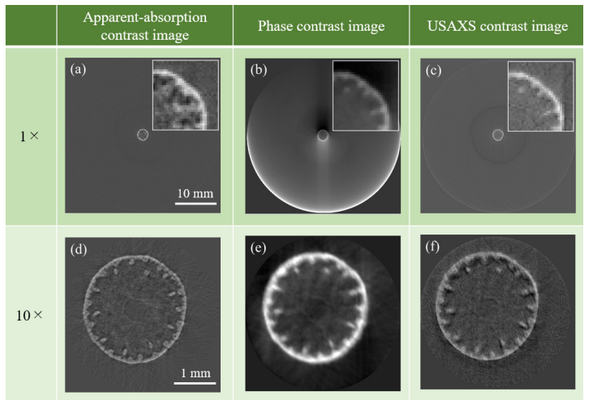

Figure 3: Reconstructed slice images of the stem of Japanese pampas grass (*Miscanthus sinensis*). The images in the left (**(a)** and **(d)**), center (**(b)** and **(e)**), and right (**(c)** and **(f)**) columns are the apparent-absorption contrast, phase contrast, and USAXS contrast images, respectively. The magnification factor is 1× for the images in the top row (**(a)–(c)**), and 10× for those in the bottom row (**(d)–(f)**). For comparison, the insets in **(a)–(c)** show digital zoom (10×) images of the upper-right part of the slice images of the sample.

REFERENCES

[1] D. Wakabayashi, Y. Suzuki, Y. Shibazaki, H. Sugiyama, K. Hirano, R. Nishimura, K. Hyodo, N. Igarashi and N. Funamori, *Rev. Sci. Instrum.* **93**, 033701 (2022).
[2] K. Hirano, H. Sugiyama, R. Nishimura, D. Wakabayashi, Y. Suzuki, N. Igarashi and N. Funamori, *J. Synchrotron Rad.* **29**, 787 (2022).
[3] N. Watanabe, T. Sasaya, Y. Imai, S. Iwata, K. Zama and S. Aoki, *AIP Conf. Proc.* **1365**, 313 (2011).

BEAMLINES

BL-14B, BL-20B and AR-NE1A

K. Hirano, D. Wakabayashi, Y. Shibazaki, H. Sugiyama, R. Nishimura, Y. Suzuki, K. Hyodo, N. Igarashi and N. Funamori (KEK-IMSS-PF)